論文 / 著書情報
Article / Book Information

Title	Epitaxial growth and electronic structure of LaTiO_x_ films
Authors	A. Ohtomo,D. A. Muller,J. L. Grazul,H. Y. Hwang
Citation	Applied Physics Letters, Vol. 80, No. 21,
Pub. date	2002, 5
URL	http://scitation.aip.org/content/aip/journal/apl
Copyright	Copyright (c) 2002 American Institute of Physics

Epitaxial growth and electronic structure of $LaTiO_x$ films

A. Ohtomo, D. A. Muller, J. L. Grazul, and H. Y. Hwang[a)]
Bell Laboratories, Lucent Technologies, Murray Hill, New Jersey 07974

(Received 15 February 2002; accepted for publication 27 March 2002)

$LaTiO_x$ films have been grown on (001) perovskite oxide substrates by pulsed-laser deposition. Both single-phase perovskite $LaTiO_3$ and layered $La_2Ti_2O_7$ films could be stabilized by varying the oxygen partial pressure and substrate temperature during growth. We have obtained a crystallographic and electronic phase diagram for $LaTiO_x$ films, demonstrating the ability to vary the titanium valence from 3+ to 4+ in thermodynamically unfavorable growth conditions by utilizing interface energies. © *2002 American Institute of Physics.* [DOI: 10.1063/1.1481767]

The physical properties of $La_{1-x}Sr_xTiO_3$ evolve from a semiconductor to an antiferromagnetic insulator as the formal titanium valence varies from 4+ to 3+ with substitutional doping.[1] For a broad range of intermediate valences, a good metal is formed, and this system is currently studied as a prototypical example of the development of a Mott–Hubbard gap as the $3d^1$ configuration at half filling is approached.[2] In the field of oxide electronics, this is an important materials family, since $SrTiO_3$ is a common substrate and doped $SrTiO_3$ is a high-mobility metallic layer, while modulating the correlation gap of $LaTiO_3$ makes it a candidate for novel electronic devices.[3,4]

The synthesis of stoichiometric bulk $LaTiO_3$ is quite difficult, primarily due to the extremely reducing conditions necessary to stabilize Ti^{3+}. For instance, the thermodynamic phase stability of Ti_2O_3 requires an oxygen partial pressure (P_{O_2}) below 10^{-10} Torr at typical growth temperatures. Pulsed-laser deposition (PLD) is potentially suitable for controlling the oxidation process during metal-oxide thin-film growth. The metal-oxide in the bulk target can be reduced during burst ablation with short laser pulses,[5] and the oxidation process on the surface of the growing film generally involves not only bulk thermodynamics (temperature and P_{O_2}), but also surface oxidation kinetics[6,7] and interface energies.[8]

In this letter, we report a systematic study controlling the crystalline phase of $LaTiO_x$ films grown on perovskite substrates. As a function of P_{O_2} during growth, either perovskite $LaTiO_3$ or the layered compound $La_2Ti_2O_7$ is formed. The microstructure of the films reflects the competition between the bulk thermodynamic oxidative state, which favors $La_2Ti_2O_7$, and the interface energy, which favors $LaTiO_3$. We demonstrate the ability to control the Ti valence between 4+ (ferroelectric band insulator $La_2Ti_2O_7$) and 3+ (Mott insulator $LaTiO_3$) far from thermodynamic limits.

$LaTiO_x$ films were grown in an ultra-high-vacuum chamber (Pascal) by PLD, using a single-phase $La_2Ti_2O_7$ polycrystalline target grown by solid-state reaction processing in air. Single-crystal (001) $SrTiO_3$ and $LaAlO_3$ substrates were used to grow 2000 Å films at temperatures between 650 and 950 °C, as measured by a pyrometer. A KrF excimer laser with a repetition rate of 5–10 Hz was used for ablation, with a laser fluence at the target surface of ~ 1.7 J/cm^2. The target–substrate distance was 45 mm, and P_{O_2} was varied between 0.1 and 10^{-10} Torr, as monitored by a residual gas analyzer on the chamber. After the growth, the temperature was lowered at a constant rate of 50 °C/min, keeping P_{O_2} constant.

Reflection high-energy electron diffraction (RHEED) intensity oscillations of the specular spot were observed at the beginning of the growth for all deposition experiments carried out on $SrTiO_3$ at growth temperatures below 850 °C and $P_{O_2} \leq 1\times10^{-4}$ Torr. Regular oscillations typically disappeared after 6–10 periods, and the pattern showed weak streaks and broad diffraction spots after the initial growth, indicating a roughening surface. With $P_{O_2} > 1\times10^{-4}$ Torr, twinned streaks with a slight tilting from the surface normal were observed for the films assigned to be $La_2Ti_2O_7$, as discussed below. From the film thickness measured by Rutherford backscattering spectroscopy (RBS), the observed RHEED oscillation period is found to correspond to the growth of one perovskite unit cell (~ 4 Å).

The epitaxial structure of the films grown both on $SrTiO_3$ and on $LaAlO_3$ in one deposition run showed essentially the same characteristics. Figure 1(a) shows the θ–2θ x-ray diffraction (XRD) pattern of a film grown at 970 °C in $P_{O_2} = 2\times10^{-4}$ Torr on $SrTiO_3$. The film is determined to be the (-210) orientation of monoclinic $La_2Ti_2O_7$ ($a = 13.01$ Å, $b = 5.54$ Å, $c = 7.81$ Å, $\beta = 98.7°$).[9] $La_2Ti_2O_7$ is derived from the perovskite structure by considering four unit-cell-thick {110} perovskite layers connected by crystallographic shears in the [100] direction, which incorporate the extra oxygen. From the epitaxial relation between the distorted TiO_6 octahedral lattice in $La_2Ti_2O_7$ with respect to the (001) perovskite lattice, the crystallographic angle between (-210) $La_2Ti_2O_7$ and (001) $SrTiO_3$ is 4.52°. Consequently, the higher-index peaks of the film are not seen for a scan aligned on axis with the $SrTiO_3$ substrate [Fig. 1(a), upper curve]. By tilting the substrate by 4.5° off axis from the surface normal along the $SrTiO_3\langle 100\rangle$ direction, the intense $La_2Ti_2O_7$ film peaks [labeled as *aligned to layer* in Fig. 1(a)] are recovered.

[a)]Electronic mail: hyhwang@lucent.com

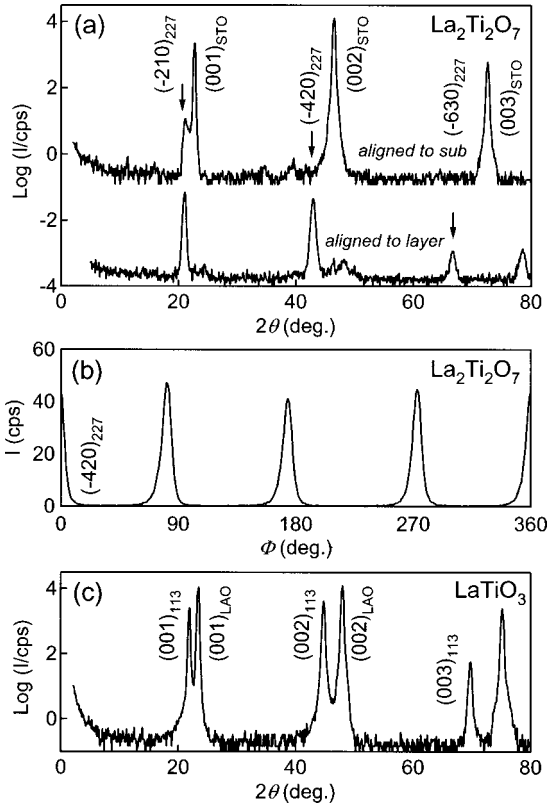

FIG. 1. (a) θ–2θ x-ray diffraction scan of a $La_2Ti_2O_7$ (227) film grown on a (001) $SrTiO_3$ (STO) substrate. Upper and lower curves were taken by aligning to the substrate (001) plane and the film (-210) plane, respectively. (b) In-plane azimuthal scan (Φ scan) of the (-420) peak for the same film shown in (a), reflecting the fourfold symmetry of vicinal grains. (c) θ–2θ scan of a $LaTiO_3$ (113) film grown on (001) $LaAlO_3$ (LAO).

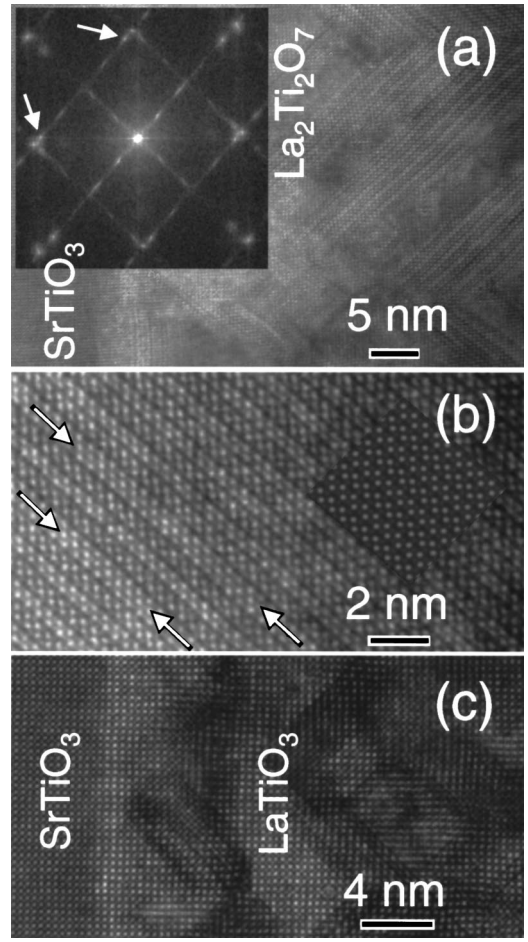

FIG. 2. Annular dark-field scanning transmission electron microscope images for $La_2Ti_2O_7$ [(a) and (b)] and $LaTiO_3$ (c) grown on (001) $SrTiO_3$ substrates taken along a $SrTiO_3$ [100] zone axis. Inset in (a) depicts a Fourier transform of the image, and the arrows indicate the tilting twin microstructure of $La_2Ti_2O_7$. Inset in (b) shows a simulated image obtained assuming the bulk structure. Stacking faults in the $La_2Ti_2O_7$ film are indicated by arrows.

The film is twinned across the $\langle 100 \rangle$ direction of the substrate; therefore, (-210) peaks have fourfold symmetry as shown by an in-plane ϕ scan for the same sample [Fig. 1(b)]. Similar XRD patterns were obtained for other films grown at $P_{O_2} \geqslant 2\times10^{-4}$ Torr. Figure 1(c) shows the θ–2θ XRD pattern of a film grown at 700 °C in $P_{O_2}=5\times10^{-9}$ Torr on $LaAlO_3$. The film shows strong peaks aligned with the substrate, assigned to be the perovskite-phase $LaTiO_3$ $(00l)$ where l is the Miller index for the pseudocubic lattice.

Figure 2 compares annular dark-field images of two films obtained by scanning transmission electron microscopy (JEOL 2010F). Figure 2(a) shows a $La_2Ti_2O_7$ film, viewed parallel to the $SrTiO_3$ substrate [100] zone axis, displaying the characteristic layered structure along the perovskite {110} directions. The different orientation grains, arising from the fourfold orientation degeneracy discussed in Fig. 1(b), are clearly seen. A Fourier transform of Fig. 2(a) [inset to Fig. 2(a)] reproduces the 4.5° tilt from the substrate normal observed in Fig. 1(a). Figure 2(b) shows a higher-magnification view of a single grain. The observed layered structure is well reproduced by the inset simulation of $La_2Ti_2O_7$, viewed along a projection that is $(\beta\text{-}90)°$ from the c-axis. This is consistent with the orientation relationship determined by XRD.

Figure 2(c) shows a $LaTiO_3$ film grown on $SrTiO_3$. Although the film clearly retains the perovskite structure of the substrate near the interface, a high density of {110} faults develops, driven energetically to achieve the equilibrium oxidative state of Ti. All of the film structures shown in Fig. 2 can be considered members of the homologous series $A_{n+1}B_{n+1}O_{3n+5}$, $0\leqslant n\leqslant\infty$, where $n=3$ corresponds to $La_2Ti_2O_7$ and $n=\infty$ corresponds to $LaTiO_3$.[9] Unlike other perovskite-derived series such as Ruddlesden–Popper phases,[10] in this structural series, the valence states of cations A and B change with n. The {110} faults in Fig. 2(c) correspond, therefore, to locally raising the oxidative state of Ti. The stacking faults seen in $La_2Ti_2O_7$, indicated by arrows in Fig. 2(b), can be considered $n=4$ $La_5Ti_5O_{17}$ interlayers, for which the Ti valence is slightly less than $4+$. The structure of the $LaTiO_3$ film is quickly dominated by the interface energy and oxidation kinetics at the growing interface, as we do not observe further evolution of the film structure above $\sim$10 perovskite unit cells.

Film composition was determined from RBS and x-ray photoelectron spectroscopy (XPS). XPS was performed in a separate analysis chamber (Perkin Elmer Φ5800) after quick *ex-situ* transfer from the growth chamber, using an Al $K\alpha$ x-ray source with an escape angle of 45°. The surface La to Ti ratio was found to be, typically, 0.99 ± 0.02, reflecting stoichiometric transfer of the target cation species. RBS mea-

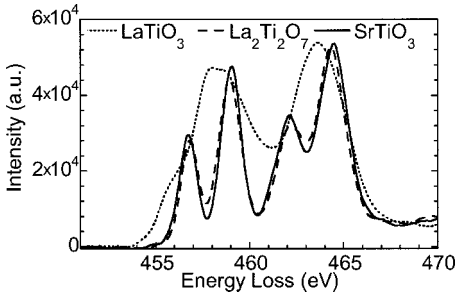

FIG. 3. Ti $L_{2,3}$ electron energy-loss spectra taken from the $LaTiO_3$ film, $La_2Ti_2O_7$ film, and $SrTiO_3$ substrate with ~ 0.7 eV energy resolution.

surements using a 2 MeV Ar^+ beam were used to estimate film stoichiometry, using the La to Ti ratio obtained from XPS. This was necessary to resolve the signal overlap of the film and substrate elements Ti and O. Simulation of the random yield spectra performed assuming the composition of La:Ti:O$=1:1:x$ yielded values of $x=3.5\pm 0.15$ and 3.0 ± 0.1 for films identified as $La_2Ti_2O_7$ and $LaTiO_3$, respectively. The channeling yield along the substrate [001] direction was quite poor, 85% for $La_2Ti_2O_7$ and 56% for $LaTiO_3$, reflecting the microstructure revealed in Fig. 2.

Evaluation of the Ti valence, as well as refining the oxygen stoichiometry, by XPS was unsuccessful due to the tendency of the surface of the film to further oxidize upon exposure to air. In order to measure the Ti valence accurately in the bulk of the film, electron energy-loss spectroscopy (EELS) measurements were performed in the electron microscope. The sample thickness was chosen so that surface states produce a negligible fraction of the transmitted signal. Figure 3 shows Ti $L_{2,3}$ edge EELS spectra taken from $LaTiO_3$ and $La_2Ti_2O_7$ films, as well as the $SrTiO_3$ substrate. The close agreement of the $La_2Ti_2O_7$ and the $SrTiO_3$ spectra confirms the $4+$ oxidative state of Ti in $La_2Ti_2O_7$. A core-level shift of ~ 1.2 eV is clearly seen for $LaTiO_3$, indicating a Ti^{3+} valence state. The observed Ti $L_{2,3}$ edge features in the EELS spectra closely match the Ti $2p$ x-ray absorption spectra reported for $La_{1-x}Sr_xTiO_3$ in bulk.[11]

Figure 4 summarizes our results in a phase diagram for $LaTiO_x$ films grown in this study. The boundary between $LaTiO_3$ and $La_2Ti_2O_7$ is located at a constant line of $P_{O_2} \sim 1\times 10^{-4}$ Torr. The films assigned to $La_2Ti_2O_7$ always showed insulating properties, while $LaTiO_3$ displayed increasingly metallic behavior with decreasing P_{O_2}. Hall-effect measurements show electron carrier densities varying from 10^{19} to 10^{22} cm^{-3} across this range, resulting from the known propensity of $LaTiO_3$ to accommodate significant oxygen off-stoichiometry.[2,12] Our results for films grown on (001) perovskite substrates can be contrasted with work on (110) substrates,[13] in which the different orientations promote the stabilization of $La_2Ti_2O_7$. Although the defect structure observed in $LaTiO_3$ indicates considerable disorder, we note that below ~ 6 unit-cell-thick $LaTiO_3$ layers can be stabilized completely free of {110} faults. This then can be considered as a functional electronic element in oxide heterostructures.

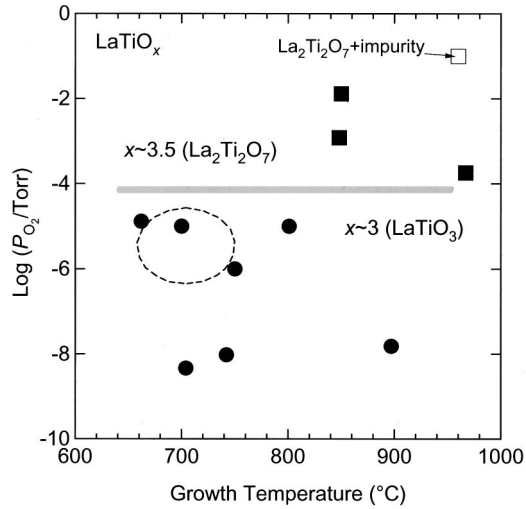

FIG. 4. Growth phase diagram of oxygen partial pressure vs growth temperature for 2000-Å-thick $LaTiO_x$ films. Samples indicated by closed circles and closed squares were evaluated to be $LaTiO_3$ and $La_2Ti_2O_7$, respectively. Dashed circle indicates the optimal growth condition for $LaTiO_3$.

The authors thank M. Siegert, D. C. Jacobson, and R. L. Opila for discussions and assistance regarding RBS and XPS. One of the authors (A.O.) acknowledges partial support by the Nishina Memorial Foundation, Japan.

[1] Y. Tokura, Y. Taguchi, Y. Okada, Y. Fujishima, T. Arima, K. Kumagai, and Y. Iye, Phys. Rev. Lett. **70**, 2126 (1993).
[2] Y. Taguchi, T. Okuda, M. Ohashi, C. Murayama, N. Mori, Y. Iye, and Y. Tokura, Phys. Rev. B **59**, 7917 (1999).
[3] D. M. Newns, J. A. Misewich, C. C. Tsuei, A. Gupta, B. A. Scott, and A. Schrott, Appl. Phys. Lett. **73**, 780 (1998).
[4] T. Hato, A. Yoshida, C. Yoshida, H. Suzuki, and N. Yokoyama, Appl. Phys. Lett. **70**, 2900 (1997).
[5] A. Gupta and B. W. Hussey, Appl. Phys. Lett. **58**, 1211 (1991).
[6] M. Hiratani, K. Imagawa, and K. Takagi, J. Appl. Phys. **78**, 4258 (1995).
[7] X. D. Zhu, W. Si, X. X. Xi, and Q. Jiang, Appl. Phys. Lett. **78**, 460 (2001).
[8] S. Surnev, G. Kresse, M. G. Ramsey, and F. P. Netzer, Phys. Rev. Lett. **87**, 086102 (2001).
[9] H. W. Schmalle, T. Williams, A. Reller, A. Linden, and J. G. Bednorz, Acta Crystallogr., Sect. B: Struct. Sci. **49**, 235 (1993).
[10] S. N. Ruddlesden and P. Popper, Acta Crystallogr. **10**, 538 (1957); **11**, 54 (1958).
[11] M. Abbate, F. M. F. de Groot, J. C. Fuggle, A. Fujimori, Y. Tokura, Y. Fujishima, O. Strebel, M. Domke, G. Kaindl, J. van Elp, B. T. Thole, G. A. Sawatzky, M. Sacchi, and N. Tsuda, Phys. Rev. B **44**, 5419 (1991).
[12] F. Lichtenberg, D. Widmer, J. G. Bednorz, T. Williams, and A. Reller, Z. Phys. B: Condens. Matter **82**, 211 (1991).
[13] J. Fompeyrine, J. W. Seo, and J.-P. Locquet, J. Eur. Ceram. Soc. **19**, 1493 (1999).